CHAPTER

# Complex Structures

# 17

## CHAPTER OUTLINE




**Physics of Condensed Matter.** DOI: 10.1016/B978-0-12-384954-0.00017-7

# 17.1 LIQUIDS

## 17.1.1 Introduction

It is well known that matter exists in three different (solid, liquid, and gaseous) phases. Solids have an ordered arrangement of atoms or molecules as evidenced by rigid and sharp Bragg reflections in a diffraction experiment. Liquids and gases are fluids and will flow even under a small shear stress. In diffraction experiments, they yield only diffuse rings, showing that there is no long arrangement of molecules. In addition, there are glasses and amorphous solids that blur the distinction between solids and fluids. The atoms or molecules in glasses are arranged at random, whereas those in amorphous solids have short-range order.

Van der Waals first pointed out the continuity of liquid and gaseous states. At low temperatures below a critical temperature, two fluid phases can coexist in equilibrium: the dense phase is called liquid, and the less-dense phase is called gas. By heating above the critical temperature, compressing, and cooling, one can pass continuously from low-temperature gas to low-temperature liquid. The difference between liquid and gas is essentially a difference in density.

For roughly spherical molecules (rare gases), there is disorder in only translational motion. There is the possibility of rotational disorder in molecules that are far from spherical. In plastic crystals, both kinds of disorder occur, whereas in "liquid crystals," there can be translational order but rotational disorder.

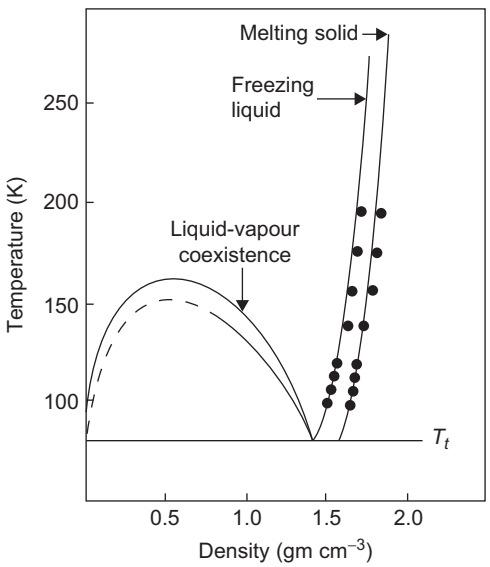


**FIGURE 17.1**

Phase diagram for the 6-12 fluid (solid lines) and for argon (dashed lines and circles). Here, $\epsilon/k = 119^\circ$ K, $\sigma = 3.405$ Å.

*Reproduced from Barker and Henderson[5] with the permission of the American Physical Society.*

## 17.1.2 Phase Diagram

The study of the physics of liquids is mainly to understand why particular phases are stable in particular ranges of density, as shown in Figure 17.1. One has to relate the stability, structure, and dynamical properties of fluid phases to

the size and shape of the molecules, atoms, or ions, and the nature of forces between them. Because the interactions that determine the bulk properties of matter are basically electrostatic in character (apart from small relativistic and retardation effects), and arise from the Coulomb interactions between nuclei and electrons, one way to predict the properties would be to solve the many-body Schrodinger equation describing the motion of nuclei and electrons. However, we will restrict the discussion to the concept of order parameters, a function that is present when order is present (solids) and vanishes when the desired order is absent (liquids).

### 17.1.3 Van Hove Pair Correlation Function

The best way to distinguish between liquids and solids is to first introduce the van Hove pair correlation function $p(\mathbf{r}_1, \mathbf{r}_2, t)$ defined as

$$p(\mathbf{r}_1, \mathbf{r}_2, t) = \left\langle \sum_{i \neq j} \delta(\mathbf{r}_1 - \mathbf{X}_i(0)) \delta(\mathbf{r}_2 - \mathbf{X}_j(t)) \right\rangle. \tag{17.1}$$

Here, $p(\mathbf{r}_1, \mathbf{r}_2, t)$ is the probability that if a particle is found at position $\mathbf{r}_1$ at time $t_1$, some other particle is to be found at position $\mathbf{r}_2$ at time $t_1 + t$. The brackets mean a thermal average, and $\mathbf{X}_i(t)$ tracks the location of the particles. Here, $\mathbf{X}_i(t)$ is the Heisenberg operator defined for all $i$ and all $t$ by the equation

$$\mathbf{X}_i(t) = e^{iHt/\hbar}\, \mathbf{X}_i e^{-iHt/\hbar}, \tag{17.2}$$

where $H$ is the Hamiltonian of the system.

The static structure factor, the dimensionless measure of scattering in a scattering experiment that measures the thermal average (because such experiments last much longer than the time scale of atomic motions), is defined as

$$S(\mathbf{q}) = \frac{1}{N} \sum_{i,j} \langle e^{i\mathbf{q}\cdot(\mathbf{X_i} - \mathbf{X_j})} \rangle. \tag{17.3}$$

Eq. (17.3) can be rewritten in the alternate form

$$S(\mathbf{q}) = \frac{1}{N} \sum_{i,j} \int d\mathbf{r}_1 d\mathbf{r}_2\, e^{i\mathbf{q}\cdot(\mathbf{r}_1 - \mathbf{r}_2)} \langle \delta(\mathbf{r}_1 - \mathbf{X}_i) \delta(\mathbf{r}_2 - \mathbf{X}_j) \rangle. \tag{17.4}$$

From Eqs. (17.1) and (17.4), we obtain

$$S(\mathbf{q}) = 1 + \frac{1}{N} \int d\mathbf{r}_1\, d\mathbf{r}_2\, p(\mathbf{r}_1, \mathbf{r}_2, 0) e^{i\mathbf{q}\cdot(\mathbf{r}_1 - \mathbf{r}_2)}. \tag{17.5}$$

We define

$$p(\mathbf{q}) = \frac{1}{V} \iint d\mathbf{r}\, d\mathbf{r}'\, p(\mathbf{r} + \mathbf{r}', \mathbf{r}, 0) e^{i\mathbf{q}\cdot\mathbf{r}'}, \tag{17.6}$$

where $V$ is the volume of the system. From Eqs. (17.5) and (17.6), we obtain

$$S(\mathbf{q}) = 1 + \frac{V}{N} p(\mathbf{q}). \tag{17.7}$$

### 17.1.4 Correlation Function for Liquids

In general, liquids are homogeneous and isotropic. Therefore, one can assume that the pair correlation function $p(\mathbf{r}_1, \mathbf{r}_2)$ will depend on the distance $r = |\mathbf{r}_1 - \mathbf{r}_2|$. If the density of the liquid is $\rho = N/V$, a dimensionless correlation function $g(r)$ can be defined as

$$g(r) = \frac{p(r)}{\rho^2}. \tag{17.8}$$

One obtains from Eqs. (17.5) and (17.8)

$$S(\mathbf{q}) = 1 + \rho \int d\mathbf{r}\, g(r) e^{i\mathbf{q}\cdot\mathbf{r}}. \tag{17.9}$$

Eq. (17.9) can be rewritten in the alternate form

$$S(\mathbf{q}) = 1 + \rho \int d\mathbf{r}\, e^{i\mathbf{q}\cdot\mathbf{r}} + \rho \int d\mathbf{r}\, [g(r) - 1] e^{i\mathbf{q}\cdot\mathbf{r}}. \tag{17.10}$$

The second term in Eq. (17.10) is a delta function, which is zero except when directly along the scattering beam. Thus, it can be dropped while analyzing the experimental results of scattering, and one obtains from Eq. (17.10)

$$S(\mathbf{q}) \approx 1 + \rho \int d\mathbf{r}\, [g(\mathbf{r}) - 1] e^{i\mathbf{q}\cdot\mathbf{r}}. \tag{17.11}$$

## 17.2 SUPERFLUID $^4$He

### 17.2.1 Introduction

Kammerlingh Onnes discovered in 1908 that liquid helium never solidified under its own vapor pressure. The interaction between the helium atoms is very weak because helium is an inert gas. The liquid phase is very weakly bound, and the normal boiling point is very low (4.2° K). The large-amplitude quantum mechanical zero-point vibrations due to the small atomic masses and the weak interactions do not permit the liquid to freeze into the crystalline state. Liquid $^4$He solidifies only when a pressure of at least 25 atmospheres is applied. Therefore, it is possible to study liquid $^4$He all the way down to the neighborhood of absolute zero.

### 17.2.2 Phase Transition in $^4$He

At 2.17° K, a remarkable phase transition was discovered in liquid $^4$He under saturated vapor pressure. When the liquid was cooled through this temperature, all boiling ceased, and the liquid became perfectly quiescent. This effect occurs because liquid helium becomes an enormously good heat conductor. The thermal inhomogeneities that give rise to bubble nucleation are absent. The specific heat versus temperature curve of liquid $^4$He was shaped like a Greek letter $\lambda$, characteristic of a

second-order phase transition. This temperature is called the lambda point, and the experimental results are shown in Figure 17.2.

The temperature at the lambda point is usually denoted by $T_\lambda$. Below this temperature, liquid $^4$He has remarkable flow as well as the "superheat" transport properties. If a small test tube containing the liquid were raised above the surrounding helium bath, a mobile film of the liquid would be transported up the inner walls. Eventually, it would drip back into the bath, and the test tube would be emptied. Kapitza (Ref. 10) showed that liquid $^4$He could flow through the tiniest pores and cracks. Allen and Jones (Ref. 10) found that if a glass tube packed tightly with a powder was partially immersed in a $^4$He bath and then heated, a fountain of helium rising high above the level of the surrounding helium bath was produced.

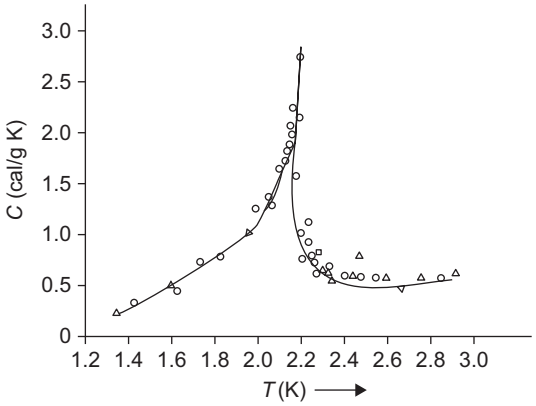


**FIGURE 17.2**

Schematic diagram of the specific heat of liquid helium versus temperature.

### 17.2.3 Two-Fluid Model for Liquid $^4$He

Landau (Ref. 10) and Tisza independently developed a two-fluid model to describe these phenomena. According to the two-fluid model, below $T_\lambda$, liquid $^4$He can be thought of as two interpenetrating fluids known as the normal and superfluid components. The superfluid component does not carry entropy and is involved in superflow through pores and cracks. In addition, it does not interact with the walls of a vessel containing the fluid in a dissipative fashion. In contrast, the normal component transports heat and exhibits viscosity, which allows transfer of energy between the liquid and the walls. The normal fluid density decreased with decreasing temperature, whereas the superfluid density increased, becoming dominant at the lowest temperature. The superfluid component replaces the normal fluid, which carries heat away from the heat source. The flow of the superfluid component toward a source of heat manifests in the fountain effect mentioned previously. The normal fluid consists of a gas of quantized thermal excitations that include the phonons (longitudinal sound waves) and rotons (short-wavelength compact excitations). It was predicted that heat transport would obey a wave equation that describes the compression and rarefactions in the proton/roton "gas," which is known as second sound.

### 17.2.4 Theory of Superfluidity in Liquid $^4$He

London (Ref. 15) noted that as the temperature of liquid $^4$He is reduced through the transition temperature, the occupancy of the one-particle ground state becomes macroscopic and can be thought of as a Bose–Einstein (BE) condensate, which is the superfluid component of the two-fluid picture, although strong interactions between the atoms in the liquid modify this picture. According to London, the superfluid atoms are governed by a wave-function-like entity called the order parameter

that was originally introduced by Ginzburg and Landau to explain the phenomenon of superconductivity (described in detail in Section 14.4.1). The order parameter $\Psi$ for a superfluid $^4$He is given by

$$\Psi = \Psi_0 e^{i\phi}, \tag{17.12}$$

where $\Psi_0$ is roughly thought of as the square root of the density of the superfluid component, and $\phi$ is a phase factor. The fact that the macroscopic order parameter is also described by a definite phase is known as broken gauge symmetry. It has been shown that the superfluid velocity is proportional to the gradient of the phase. The macroscopic order parameter picture describes how the helium atoms march in "lock step" during superfluid flow. The existence of quantized vortices in superfluid $^4$He is also a consequence of this model. In fact, this phenomena is also seen in superfluid liquid $^3$He (to be discussed in the next section) and in superconductivity in solids, where a quantized current vortex must enclose a quantum of flux (discussed in Chapter 14).

The fundamental assumption that underlies the modern theory of superfluidity in a Bose system such as liquid $^4$He is that the superfluid phase is characterized by a generalized Bose–Einstein Condensation (BEC). We assume that at any given time $t$, it is possible to find a complete orthonormal basis (which may itself depend on time) of single-particle states such that one and only one of these states is occupied by a finite fraction of all the particles, while the number of particles in any other single-particle state is of order 1 or less. The corresponding single-particle wave function $\chi_0(r,t)$ is called a condensate wave function, and the $N_0$ particles occupying it, the condensate. The $T = 0$ condensate fraction $N_0/N \sim 0.1$, where $N$ is the total number of particles in the system. The macroscopic occupation occurs only in a single-particle state because according to the Hartree–Fock approximation, the macroscopic occupation of more than one state is always energetically unfavorable provided the effective low-energy interaction is repulsive, as is the case for $^4$He.

Because the BEC occurs in the sense defined earlier, at any given time there exists one and only one single-particle state $\chi_0(r,t)$ that is macroscopically occupied, and the conceptual basis for superfluidity is quite simple. We can write

$$\chi_0(r,t) = |\chi_0(r,t)|e^{i\phi(r,t)} \tag{17.13}$$

and define the superfluid velocity $v_s(r,t)$ by

$$v_s(r,t) \equiv \frac{\hbar}{m}\nabla\phi(r,t), \tag{17.14}$$

from which we obtain

$$\nabla \times v_s = 0. \tag{17.15}$$

Thus, the superfluid flow is irrotational. In addition, because no "ignorance" is associated with the single state $\chi_0$, the entropy must be carried entirely by the "normal" component, i.e., the particles occupying single-particle states other than $\chi_0$. These two observations provide the basis for Landau's phenomenological two-fluid hydrodynamics. However, the superfluid density $\rho_s$, which occurs in the latter, is given by $(T \to 0)\ \rho_s \to N/V$ while $N_0 \to 0.1\,N$.

In a region where $|\chi_0|$ is everywhere nonzero, the application of the Stokes theorem to the curl of Eq. (17.14) leads to the conclusion that the integral of $v_s$ around any closed curve is zero (Problem 17.1). However, we consider a line or a region infinite in one dimension on which $|\chi_0(r,t)|$

vanishes. This would happen if the liquid is physically excluded from this region, or while atoms are present in this region, the single-particle state into which BEC has taken place happens to have a nodal line there. When we integrate Eq. (17.14) around a circuit that encloses the one-dimensional region, the fact that the phase of the wave function $\chi_0$ must be single-valued modulo $2\pi$ leads to the Onsager–Feynman quantization condition (Problem 17.2)

$$\oint v_s \cdot dl = nh/m. \tag{17.16}$$

In a simply connected region of space, Eq. (17.16) can be satisfied by a "vortex," which is a pattern of flow in which $v_s \sim 1/r$, where $r$ is the perpendicular distance from the "core." Because $|\chi_0|$ vanishes at $r = 0$, $v_s$ is not defined, and hence, the singularity that appears at the core is physically irrelevant.

Thus, in a superfluid system, the circulation is quantized according to Eq. (17.16). In practice, the values $n = \pm 1$ are of interest because vortices with higher values of $n$ are unstable against decay into these. However, vortices can be metastable for astronomical times even under equilibrium conditions.

We note that the superfluid velocity $v_s(r,t)$ is not a directly observable quantity, whereas the mass current $J(r,t)$ is observable. Landau (Refs. 10-13) showed in his phenomenological theory that in stable or metastable equilibrium, this quantity is given by

$$J(r,t) = \rho_s v_s(r,t) + \rho_n v_n(r,t), \tag{17.17}$$

where the "superfluid" and "normal" densities $\rho_s$ and $\rho_n \equiv \rho - \rho_s$ are functions of only the temperature. The normal velocity $v_n(r,t)$ is assumed to behave like the velocity of a normal (nonsuperfluid) liquid. In equilibrium, $v_n(r,t)$ should be zero in the frame of reference in which the walls of the vessel are at rest.

In the 70 years since Landau's original proposal, although there has been almost universal belief that the key to superfluidity in liquid $^4$He is the onset of BEC at the lambda temperature, it has proved very difficult to verify the latter phenomenon directly. The main evidence comes from the high-energy neutron scattering and from the spectrum of atoms evaporated from the surface of the liquid. Although both are consistent with the existence of a condensate fraction of approximately 10%, neither can be said to establish it beyond all possible doubt.

## 17.3 LIQUID $^3$He

### 17.3.1 Introduction

$^3$He is a rare isotope of helium that occurs in both solid and liquid states. Because the nuclear moments are very small, solid $^3$He undergoes nuclear magnetic ordering at a temperature of about 1 mK. Therefore, in the range of temperatures above 0.01° K, the nuclear spins of the $^3$He atoms comprised of the solid are almost fully disordered. Hence, for spin 1/2 nuclei, the entropy $S_{solid} = R \ln 2$ per mole (Problem 17.3). In contrast, liquid $^3$He obeys Fermi–Dirac statistics. Well below the Fermi degeneracy temperature $(T_F)$, which is less than 1° K, both the specific heat and the entropy will be linear functions of the temperature, $S_{liquid} = \gamma T$. The liquid–solid phase equilibrium is determined by the Clausius–Clapeyron equation, according to which the melting curve is given by

$$\frac{dP}{dT} = \frac{S_{liquid} - S_{solid}}{V_{liquid} - V_{solid}} = \frac{Latent\ Heat}{T(V_{liquid} - V_{solid})}. \tag{17.18}$$

For $^3$He because $V_{liquid} > V_{solid}$, the denominator is always positive. In the Fermi degenerate region (at the lowest temperatures), $S_{liquid} < S_{solid}$ and hence the slope of the melting curve becomes negative; i.e., *it takes heat to freeze liquid* $^3$He.

### 17.3.2 Possibility of Superfluidity in Liquid $^3$He

In 1972, Osheroff, Richardson, and Lee (Ref. 20) and Osheroff, Gully, Richardson, and Lee[21] discovered that liquid $^3$He possesses three anomalous phases below 5 mK, each of which appears to display most of the properties expected of a superfluid. Because liquid $^3$He obeys Fermi rather than Bose statistics, the mechanism of superfluidity cannot be simple BEC as in liquid $^4$He. It is believed that just as in metallic superconductors, the fermions pair up to form "Cooper pairs," which are sort of giant diatomic quasimolecules of which the characteristic "radius" is much larger than the typical interatomic distance. These molecules, which are composed of two fermions, effectively obey Bose statistics and hence can undergo BEC. We will discuss superfluidity in liquid $^3$He in the next section.

The strong short-range repulsion of the quasiparticles in liquid $^3$He prevents pairing through Cooper pairs that have zero angular momentum $(l = 0)$ so that the members of a pair do not rotate around one another. However, over the years, a number of higher orbital angular momentum pairing states for a hypothetical superfluid state of liquid $^3$He were proposed. It is interesting to note that both $p$-wave ($l = 1$) and $d$-wave ($l = 2$) states of relative orbital angular momentum were proposed. However, the proposals for $p$-wave pairing by Anderson and Morel (Ref. 1) and Bailan and Werthamer (Ref. 4) were later identified as the actual superfluid phases of liquid $^3$He. The basic characteristics of the hypothetical superfluid $^3$He were that (1) there would be an intrinsic pairing mechanism not mediated by an ionic lattice (phonons), and (2) the resulting Cooper pairs would have internal degrees of freedom. These properties would distinguish superfluid $^3$He from superfluid $^4$He and superconducting electrons.

### 17.3.3 Fermi Liquid Theory

Liquid $^3$He is composed of neutral atoms with nuclear spin angular momentum of $\hbar/2$ and a nuclear magnetic moment. The $^3$He atom has an odd number of elementary particles, so it obeys Fermi–Dirac statistics and the Pauli exclusion principle. Because the atoms in the liquid interact strongly, Landau developed the Fermi liquid theory (Section 7.9) to explain the properties of liquid $^3$He. The basic idea of the Fermi liquid theory is to consider the excitations of the strongly interacting system instead of concentrating on the nature of the ground state. The scattering rate of the fermions is considerably reduced due to the Pauli exclusion principle. Landau termed the excitations, which act like particles, as quasiparticles. The various properties of normal liquid $^3$He qualitatively resembled the properties of ideal Fermi gas, but the numerical factors were obtained from the Fermi-liquid parameters (Section 7.9.3). In a Fermi liquid at low temperatures, the thermally excited quasiparticles occur in a narrow band near the Fermi surface with energy width on the order of $k_BT$. Only the quasiparticles in this narrow band participate in scattering or in thermal excitations. The width of the band shrinks as $T$ is lowered, and fewer quasiparticles can participate in such events. Consequently, the specific heat $C$ and the entropy $S$ depend linearly on the temperature ($C = \alpha T$), and the mean free path is proportional to $T^{-2}$. The thermal conductivity has a $1/T$ dependence, and the viscosity has a $1/T^2$ dependence. At the lowest temperatures in a Fermi

liquid, the collisions are absent, and ordinary sound, which is produced as a result of propagation of waves of compression and rarefaction brought about by collisions of the molecules, dies away. This new mode of sound propagation is known as the *zero sound* and arises at the lowest temperatures due to self-consistent rearrangements of quasiparticles under the influence of Fermi-liquid interactions.

### 17.3.4 Experimental Results of Superfluidity in Liquid $^3$He

The classical experiment to find superfluidity in $^3$He was performed by Osheroff, Richardson, and Lee (Ref. 20) who used a Pomerchunk cell to observe two phase transitions (denoted as $A$ and $B$) at temperatures $T_A \approx 2.7$ mK and $T_B \approx 2.1$ mK, respectively. They originally misinterpreted the results as a second-order magnetic phase transition in solid $^3$He. However, subsequent nuclear magnetic resonance experiments made at the suggestion of Gully (Osheroff, Gully, Richardson, and Lee[21]) showed that the $A$ and $B$ phases were both superfluid phases of liquid $^3$He. In addition, it was observed that the $A$ phase split into two phases ($A$ and $A_1$) in a magnetic field, whereas at about 0.6 Tesla, the $B$ phase no longer existed. The early specific-heat measurements of liquid $^3$He near the superfluid transition were done by Webb et al.[26] and are shown in Figure 17.3. The shape is characteristic of a BCS pairing transition.

The phase diagram of liquid $^3$He in a magnetic field was investigated by Paulson et al.[22] at pressures below melting pressures; they studied the static magnetization of the liquid via SQUID interferometry. The $A$ phase narrowed and finally vanished at a point called the polycritical point (PCP) at about 22 bar. In a larger magnetic field, the $B$ phase is suppressed in favor of the $A$ phase even at the lowest pressure, and the PCP disappears, as shown in Figure 17.4.

A schematic P-T-H diagram showing the general topology of the superfluid phases, $A$, $A_1$, and $B$ of liquid $^3$He, is shown in Figure 17.5. The $A_1$ phase occurs between the surfaces labeled $A_1$ and $A_2$. The $A$ phase occurs at temperatures below the boundary labeled $A_2$. The boundary between phases $A$ and $B$ is labeled $B$. The surface labeled $S$ corresponds to the melting curve.

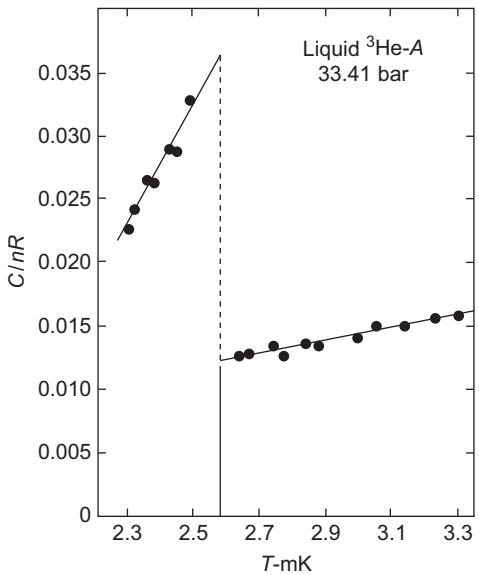


**FIGURE 17.3**

Specific-heat measurements of liquid $^3$He near the superfluid transition.

*Reproduced from Webb et al.[26] with the permission of the American Physical Society.*

### 17.3.5 Theoretical Model for the $A$ and $A_1$ Phases

The $^3$He $A$ phase corresponds to the $p$-wave equal spin pairing state first considered by Anderson and Morel.[1] It is a $p$-wave pairing state with total $L = 1$ and $S = 1$. It is an orbital

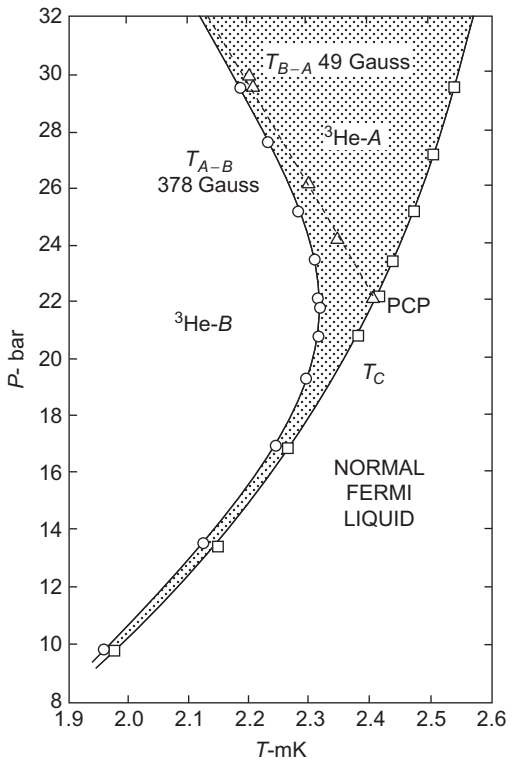


**FIGURE 17.4**

Experimental data for the phase diagram in a magnetic field.

*Reproduced from Paulson et al.[22] with the permission of the American Physical Society.*

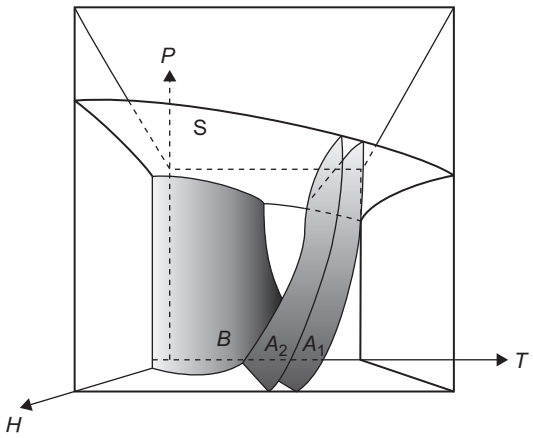


**FIGURE 17.5**

A schematic P-T-H diagram showing the superfluid phases, $A$, $A_1$, and $B$ of liquid $^3$He.

*Reproduced from Lee[14] with the permission of the American Physical Society.*

$m$ state along some direction $\hat{l}$ and spin $m = 0$ state along direction $\hat{d}$, where $\hat{d}$ is the direction of zero spin projection. The Anderson–Morel order parameter (Ref. 1) can be expressed as

$$\psi_{AM} = (orbital\ part) \times (spin\ part). \qquad (17.19)$$

Here, the orbital part is in momentum space, and the spherical harmonic $Y_{11} \sim e^{i\varphi} \sin\theta$ defines a polar axis corresponding to the direction of the pair orbital angular momentum. Thus, the Anderson–Morel order parameter (Ref. 1) can be defined as

$$\psi_{AM} \sim e^{i\varphi} \sin\theta \left[\frac{1}{\sqrt{2}}(\downarrow\uparrow + \uparrow\downarrow)\right], \qquad (17.20)$$

where the spherical harmonic $Y_{11} \sim e^{i\varphi} \sin\theta$ defines a polar axis $\hat{l}$ corresponding to the direction of the pair orbital angular momentum. Because in the spin-triplet pair-wave function, the spin part appears along the $\hat{d}$-axis, only the $(\downarrow\uparrow + \uparrow\downarrow)$ component occurs. The three-dimensional representation of the Anderson–Morel order parameter is shown in Figure 17.6a. The vector $\hat{l}$ defines the axes of the order parameter. The amplitude is zero along this axis, which corresponds to $\sin\theta$ dependence where $\theta$ is the polar angle with respect to $\hat{l}$. The vector $\vec{d}$ has the same direction for all points on the Fermi surface. The shaded region in Figure 17.17b shows the anisotropic energy gap and the two nodes along $\hat{l}$.

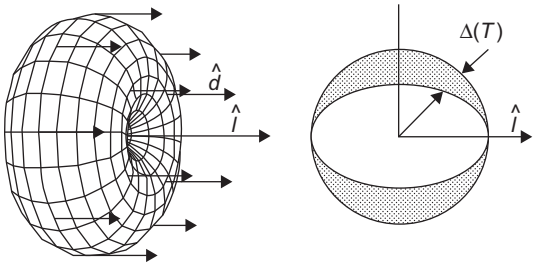


**FIGURE 17.6**

(a) A three-dimensional representation of the Anderson–Morel order parameter; (b) the anisotropic energy gap is indicated by the shaded region.

*Reproduced from Lee[14] with the permission of the American Physical Society.*

It can be shown by using a classical argument that the dipolar interaction combined with spontaneously broken symmetry would favor the state for which $\hat{l} \| \hat{d}$ (Problem 17.4). The order parameter has nodes at $\theta = 0$ and $\theta = \pi$. Because the behavior of the BCS energy gap follows the order parameter, the gap nodes also appear at $\theta = 0$ and $\theta = \pi$, which is shown in Figure 17.6b. The three-dimensional picture is obtained by a revolution about the $\hat{l}$-axis. The direction of $\hat{l}$, which is perpendicular to the walls of the container, is also sensitive to flow and to the magnetic field.

The spin state in Eq. (17.20) can be rotated in spin space, which results in the equal spin pairing version of the Anderson–Morel order parameter,

$$\psi_{AM} \sim e^{i\varphi} \sin\theta[(|\uparrow\uparrow\rangle + e^{i\Phi}|\downarrow\downarrow\rangle)], \tag{17.21}$$

where $\Phi$ is a phase factor. The $A_1$ phase has the orbital properties described by the Anderson–Morel state but has only $|\uparrow\uparrow\rangle$ spin pairs.

The concept of spin fluctuation effect was introduced earlier by Layzer and Fay, who noted that because the nuclear magnetic susceptibility of liquid $^3$He was much higher than that of an ideal Fermi gas of comparable density, there was some tendency for the liquid to be ferromagnetic. When a $^3$He quasiparticle passed through the liquid, it would polarize spins of neighboring quasiparticles parallel to its own spin because of this ferromagnetic tendency. Anderson and Brinkman[2] showed that the spin fluctuation feedback effect could indeed lead to a stable Anderson–Morel phase in a zero magnetic field. After this paper, the Anderson-Morel phase was known as the Anderson–Brinkman–Morel (ABM) phase.

### 17.3.6 Theoretical Model for the *B* Phase

The simplest Balian–Werthamer (BW) state (Ref. 4) is the $^3P_0$ state, represented by

$$\psi_{BW} \sim Y_{1,-1}|\uparrow\uparrow\rangle + Y_{10}|\uparrow\downarrow + \downarrow\uparrow\rangle + Y_{11}|\downarrow\downarrow\rangle. \tag{17.22}$$

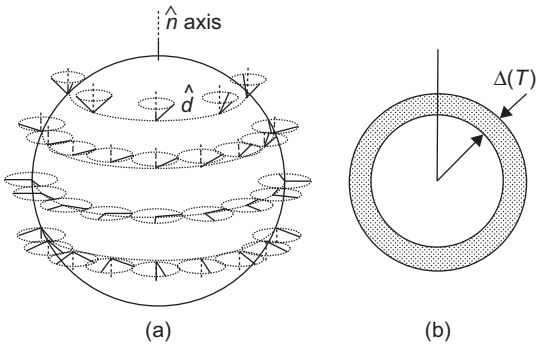


**FIGURE 17.7**

(a) The order parameter for superfluid $^3$He B; (b) the isotropic energy gap of the BW order parameter.

*Reproduced from Lee[14] with the permission of the American Physical Society.*

Because $J = 0$ for the $^3P_0$ state, the BW state is specified in terms of the vector $\hat{d}(k) = a\hat{k}$, where $a$ is a constant. The order parameter for superfluid $^3$He B showing $\hat{d}$ vectors (thick lines) rotated by 104° (Problem 17.4) about a vector along the radial directions (thin lines) for all points on the Fermi sphere is shown in Figure 17.7a. Figure 17.7b shows the isotropic energy gap of the BW order parameter.

## 17.4 LIQUID CRYSTALS

### 17.4.1 Introduction

Liquid crystal is a state of matter intermediate between that of an isotropic liquid and a crystalline solid. Liquid crystals have many of the properties of a liquid, such as high fluidity, formation and coalescence of droplets, and inability to support shear. They are also similar to crystals in the sense that they exhibit anisotropy in electric, magnetic, and optical properties. There are two broad types of liquid crystals. Liquid crystals that are obtained by melting a crystalline solid are called thermotropic where temperature and (secondarily) the pressure are the controllable parameters. Liquid crystalline behavior is also found in certain colloidal solutions and certain polymers. This type of liquid crystal is called lyotropic, for which concentration and (secondarily) the temperature are the controllable parameters.

Liquid crystals are found among certain organic compounds that may be of a variety of chemical types. However, the molecules forming liquid crystal phases have certain structural features that can be summarized as follows:

**a.** The molecules are elongated and have flat segments, as in benzene rings.
**b.** The long axis of the molecule is defined by a fairly rigid backbone containing double bonds.
**c.** The molecule should have strong dipoles and easily polarizable groups.
**d.** The extremities of the molecules are not very important.

### 17.4.2 Three Classes of Liquid Crystals

Para-azoxyanisole (PAA) and 2-*p*-methoxybenzylidene *n*-butylaniline (MBBA), the two liquid crystals that have been extensively studied, are shown in Figure 17.8.

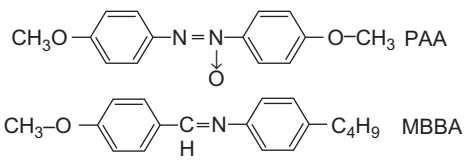


**FIGURE 17.8**

Molecular structure of para-azoxyanisole (PAA) and 2-*p*-methoxybenzylidene *n*-butylaniline (MBBA).

*Reproduced from Stephen and Straley[25] with the permission of American Physical Society.*

Liquid crystals are divided into three main classes: (a) nematic, (b) cholesteric, and (c) smectic phases. They are shown in Figure 17.9.

**(a) Nematics:** In the nematic phase, the long planar molecules are symbolized by ellipses. The long axes of the molecules align along a preferred direction, which indicates that there is a long-range orientational order. The locally preferred direction usually varies throughout the medium in the strained nematic. One defines a vector field **n(r)**, known as the director, which gives its local orientation. Its magnitude is taken

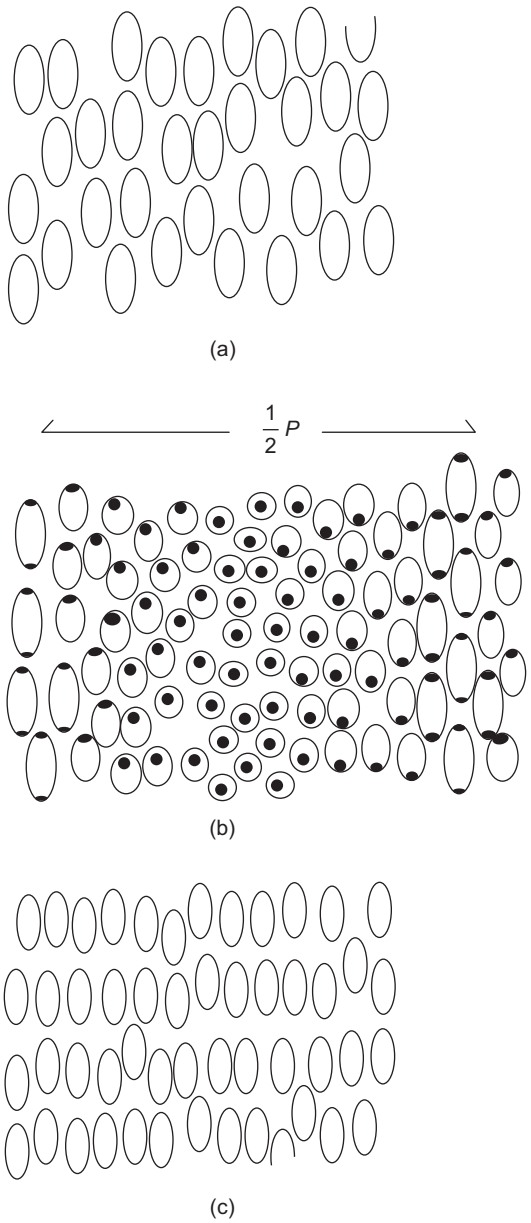


**FIGURE 17.9**

The arrangement of molecules in the (a) nematic, (b) cholersteric, and (c) smectic A phase.

*Reproduced from Stephen and Straley[25] with the permission of the American Physical Society.*

as unity. The director field can be aligned by electric and magnetic fields and by surfaces that have been properly prepared. Some structural perturbations appear as threads on optical examinations, which indicate that there is no idealized equilibrium configuration.

There is short-range order in nematics as in ordinary liquids, but no long-range order in the centers of mass of the molecules. There is no preferential arrangement of the two ends of the molecules if they differ, but they can rotate about their long axes. Thus, the sign of the director has no physical significance, and optically, a nematic behaves as a uniaxial material with a center of symmetry, which is confirmed by the absence of ferroelectric phenomena. It has been suggested on the basis of X-ray and optical data that there exists another type of nematic phase, known as the cybotactic phase. In this phase, the molecules are arranged in groups such that the centers of mass of the molecules in each group lie in a plane.

**(b) Cholesterics:** The cholesteric phase differs from the nematic phase in the sense that the director **n** varies in direction in the medium in a regular way. If a nematic initially aligned along the *y*-axis is twisted about the *x*-axis, a cholesteric configuration would be obtained. The director and the Fresnel ellipsoid rotate as one proceeds along the twist axis. The long axes of the molecules tend to align along a single preferred direction in any plane perpendicular to the twist axis. However, in a series of equidistant parallel planes, the preferred direction rotates as shown in Figure 17.9b. The distance measured along the twist axis over which the director rotates through a full circle is known as the pitch ($P$) of the cholesteric. Because **n** and –**n** are indistinguishable, the periodicity length of the cholesteric is $P/2$. The pitch of cholesterics, which is sensitive to temperature flow, chemical composition, and applied magnetic or electric fields, is comparable with visible light because it is of the order of several thousand angstroms.

The characteristic colors of the cholesterics in reflection (through Bragg reflection by the periodic structure) and their very large optical rotatory power are due to the spiral arrangement.

**(c) Smectics:** The molecules in the smectics are arranged in layers, and in addition to orientational layering, they exhibit orientational ordering. There are a number of different classes of smectics, which are briefly listed here:

**Smectic A:** In this phase, the molecules are aligned perpendicular to the layers, but there is no long-range crystalline order within a layer (see Figure 17.9c). The layers can slide freely over one another.
**Smectic B:** In this phase, there is a hexagonal crystalline order within the layers. The layers can slip on each other but cannot rotate on each other.
**Smectic C:** In this phase, the preferred axis is not perpendicular to the layers so that the phase has biaxial symmetry.
**Smectic D:** Optically, the D phase appears to have a cubic structure, and the X-ray patterns are consistent with a cubic packing.
**Smectic E:** The X-ray patterns obtained from the smectic E phase show the presence of a layered structure and a high degree of order arrangement within the planes.

### 17.4.3 The Order Parameter

If we assume that the molecules of a nematic or cholesteric liquid crystal are rigid and rodlike in shape, then we can describe the orientation of the $i$th molecule by introducing a unit vector $\overrightarrow{v}^{(i)}$ along its axis. $\overrightarrow{v}^{(i)}$ is different from the director $\mathbf{n}$, which gives the average preferred direction of the molecules. It is not possible to introduce a vector order parameter for liquid crystals, which possess a center of symmetry due to which the average of $\overrightarrow{v}^{(i)}$ vanishes. Hence, the order parameter can be expressed only as a second-rank tensor

$$S_{\alpha\beta}(\mathbf{r}) = \frac{1}{N}\sum_i \left(v_\alpha^{(i)} v_\beta^{(i)} - \frac{1}{3}\delta_{\alpha\beta}\right), \tag{17.23}$$

where the sum is over all the $N$ molecules in a macroscopic volume located at $\mathbf{r}$, and the $v_\alpha$ are the components of $\overrightarrow{v}$ referred to by a set of laboratory-fixed axes. $S_{\alpha\beta}$ is a symmetric traceless tensor of rank two and has five independent components. In the isotropic case, where the molecules have random orientation, $S_{\alpha\beta} = 0$ (Problem 17.5).

To express the order parameter for nonlinear rigid molecules, one can introduce a Cartesian coordinate system $x'y'z'$ fixed in the molecules. In the case of a uniaxial liquid crystal, the order parameter tensor is defined by

$$S_{\alpha'\beta'}(\mathbf{r}) = <\cos\theta_{\alpha'}\cos\theta_{\beta'} - \frac{1}{3}\delta_{\alpha'\beta'}>, \tag{17.24}$$

where $\cos\theta_{\alpha'}$ is the angle between the $\alpha'$ molecular axis, and the preferred direction or the optic axis. The angle brackets indicate an average over the molecules in a small but macroscopic volume. It can be shown that Eq. (17.24) is equivalent to Eq. (17.23) in the case of linear molecules or molecules with a well-defined long axis about which they rotate rapidly (Problem 17.6).

In real liquid crystals, different parts of the molecules might have to be described by different $S_{\alpha\beta}$ tensors. It is preferable to define the order parameter through a macroscopic property such as the anisotropy in the diamagnetic susceptibility,

$$Q_{\alpha\beta} = \chi_{\alpha\beta} - \frac{1}{3}\delta_{\alpha\beta}\chi_{\gamma\gamma}, \tag{17.25}$$

where $\chi_{\alpha\beta}$ is the magnetic susceptibility tensor per unit volume. By convention, repeated indices are to be summed over. Here, $Q_{\alpha\beta}$ is a symmetric traceless tensor of rank two and has five independent components.

The diamagnetic susceptibility is approximately the sum of the susceptibilities of individual molecules. We choose the principal susceptibilities of a rigid molecule to be $\chi_1^{(0)}$, $\chi_2^{(0)}$, and $\chi_3^{(0)}$, and choose the fixed axes $x'$, $y'$, and $z'$ of the molecule to coincide with the principal axes of the susceptibility. It can be easily shown for a uniaxial liquid crystal (Problem 17.7),

$$Q_{xx} = Q_{yy} = 2N[(S_{y'y'} + S_{z'z'})\chi_1^{(0)} + (S_{z'z'} + S_{x'x'})\chi_2^{(0)} + (S_{x'x'} + S_{y'y'})\chi_3^{(0)}] \tag{17.26}$$

and

$$Q_{zz} = N(S_{x'x'}\chi_1^{(0)} + S_{y'y'}\chi_2^{(0)} + S_{z'z'}\chi_3^{(0)}), \tag{17.27}$$

where $N$ is the number of molecules per unit volume. Further, it can be easily shown that

$$S_{x'x'} + S_{y'y'} + S_{z'z'} = 0. \tag{17.28}$$

Hence, there are only two independent parameters on the right side of Eqs. (17.26) and (17.27).

### 17.4.4 Curvature Strains

There is a preferred axis along which the molecules orient themselves in the microscopic region of a liquid crystal. The direction of this axis varies from place to place in equilibrium, and it can also be forced to vary by external forces. The relative orientations away from the equilibrium position are known as curvature strain, and the restoring forces are known as curvature stresses. The free energy density is a quadratic function of the curvature strains. The theory of the curvature elastic energy is based on the symmetry properties of the liquid crystal.

The three distinct curvature strains of a liquid crystal are shown in Figure 17.10 by assuming that $\hat{n}(\mathbf{r})$ is a unit vector giving the direction of the preferred orientation at the point $\mathbf{r}$ and varies slowly from point to point in molecules with permanent dipole moments. At $\mathbf{r}$, we introduce a coordinate system with $z$ parallel to $\mathbf{n}$. The curvature has six components, resulting in three curvature strains: splay, twist, and bend.

### 17.4.5 Optical Properties of Cholesteric Liquid Crystals

The unusual optical properties of cholesteric liquid crystals include the color effects seen in reflection under white light. These effects are due to the interactions of the light with the twisted arrangement of the molecules as well as the spatial variation of the dielectric constant. The variation of the dielectric constant through the medium is small ($\Delta n/n \sim 0.03$), and we will assume that the normal form of the waves propagating through the medium is approximately that of ordinary circularly

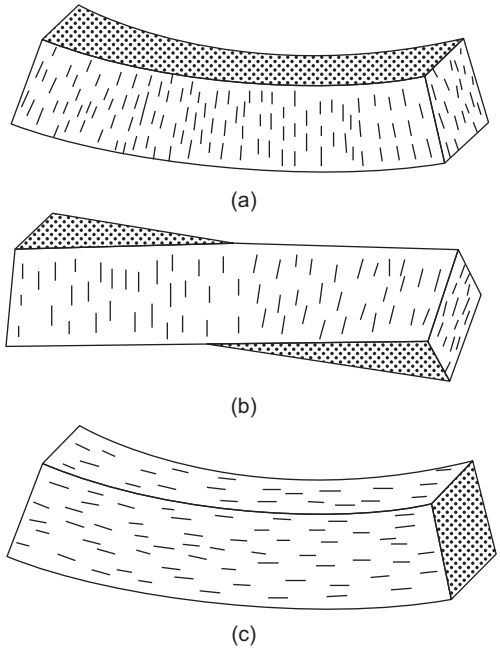


**FIGURE 17.10**

The three curvature strains of liquid crystals: (a) splay: $s_1 = \partial n_x/\partial x$, $s_2 = \partial n_y/\partial y$; (b) twist: $t_1 = -\partial n_y/\partial x$, $t_2 = \partial n_x/\partial y$; (c) bend: $b_1 = \partial n_x/\partial z$, $b_2 = \partial n_y/\partial z$.

*Reproduced from Stephen and Straley[25] with the permission of the American Physical Society.*

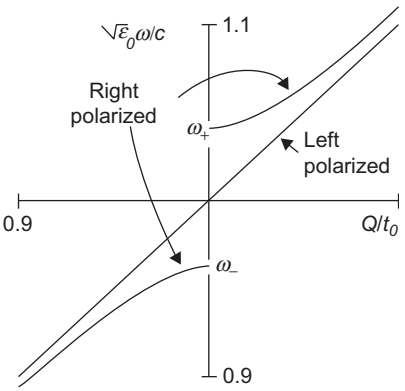


**FIGURE 17.11**

Dispersion of light in a right-hand twisting cholesteric.

*Reproduced from Stephen and Straley[25] with the permission of the American Physical Society.*

polarized waves. These waves would be strongly affected only if the half-wavelength nearly matches the periodicity length (or its projection on the wave vector) and if the sense of its rotation is the same as the twisted structure. Otherwise, the effect on the dispersion relation of the wave would be the same as in other periodic structures. Because **n** and –**n** are indistinguishable, the periodicity is one-half the pitch, and according to the Bragg formula, a "band gap" would appear at a matching wavelength

$$\lambda_0 = p \sin\theta, \tag{17.29}$$

where $p$ is the periodicity length. The periodic perturbation determines the size of the band gap. The form of the dispersion relation is shown in Figure 17.11. The right-hand circularly polarized wave is strongly affected when its half-wavelength nearly matches the periodicity length. The left-hand circularly polarized wave of the same wavelength is unaffected.

The extrema of the band gaps are obtained from the fact that light of wavelength $\lambda_0$ can travel at two distinct speeds with its electric vector aligned with the principal axes of the dielectric constant. Thus, the extrema of the band gap are

$$\begin{aligned} \omega_+ &= 2\pi c/n_-\lambda_0, \\ \omega_- &= 2\pi c/n_+\lambda_0. \end{aligned} \tag{17.30}$$

Here, $n_+$ and $n_-$ are the refraction indices. If light of frequencies between $\omega_+$ and $\omega_-$ and of the appropriate circular polarization to match the twist is directed at the liquid crystal, it is

totally reflected, and the polarization of the reflected light matches the sense of the twist. Thus, a right-hand cholesteric reflects right-polarized light, whereas left-polarized light suffers only weak reflection. Because the reflected band is narrow ($\Delta\omega/\omega \sim \Delta n/n \sim 0.03$), a pure color is reflected; this color depends on the pitch as well as the angle of incidence.

Liquid crystals are extensively used in fiber-optic devices applied in telecommunication circuits. The optics of liquid-crystal devices (LCD) has evolved extensively in the past decade.

## 17.5 QUASICRYSTALS

### 17.5.1 Introduction

It had been generally accepted among solid state physicists that crystals can have translational periodicity as well as one-, two-, three-, four-, and six-fold rotational symmetries. However, five-fold rotational symmetry could not exist in equilibrium-condensed phases. An icosahedron, which is the most locally densely packed arrangement, had been observed in liquids and amorphous solids. It was thought that an icosahedral rotational symmetry contradicts the translational periodicity and is unlikely to be found.

### 17.5.2 Penrose Tiles

Penrose introduced the concept of two-dimensional tiles in 1974 (the concept was published in 1977)[23]; he proposed that it is possible to cover (tile) any flat two-dimensional space with only two different tile shapes (known as fat and skinny rhombus) in an infinite number of aperiodic ways. The tiles, which are rhombi, must be placed such that the matching arrows are always adjacent. The Penrose tiles are shown in Figure 17.12. The smaller angle of the fat rhombus is $2\pi/5$, and the smaller angle of the skinny rhombus is $\pi/5$. If the length of each side is 1, the long diagonal of the fat rhombus (dashed line) has length $\tau = (\sqrt{5}+1)/2$, and the short diagonal of the skinny rhombus (dashed line) has length $1/\tau$.

The Penrose lattice is obtained by tiling a plane using a collection of the two Penrose tiles. The Penrose lattice, shown in Figure 17.13, shows the local regions of five-fold symmetry.

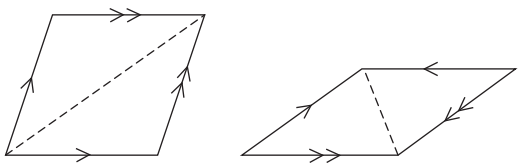

**FIGURE 17.12**
Penrose tiles.

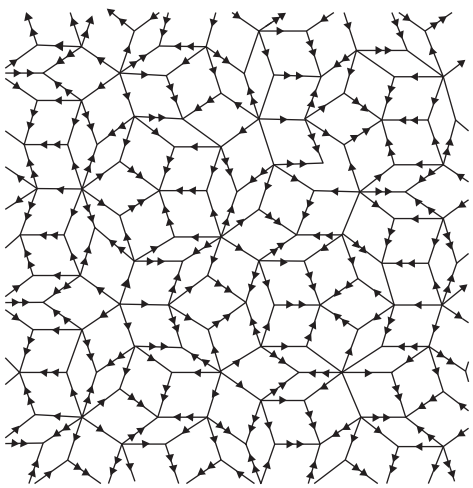

**FIGURE 17.13**
The Penrose lattice.

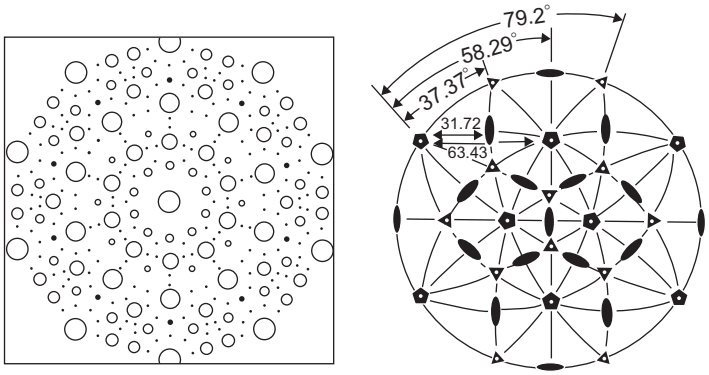


**FIGURE 17.14**

Diffraction pattern of five-fold symmetry (area proportional to the intensity) and stereogram of the icosahedral group.

*Reproduced from Misra[18] with the permission of Elsevier.*

### 17.5.3 Discovery of Quasicrystals

In 1984, Shectman et al. (Ref. 24) discovered sharp diffraction patterns of icosahedral symmetry in Al-Mn alloy rapidly quenched from the melt. The icosahedral phase in rapidly solidified Al-Mn alloy is resistant to crystallization up to 350° C and is metastable. The results of Shectman et al. are shown schematically in Figure 17.14.

In view of the above, Levine and Steinhardt generalized the notion of crystal to include a quasiperiodic translational order and named it "quasicrystal." A quasicrystal has long-range quasiperiodic order as well as long-range crystallographically forbidden orientation symmetry. The classes of quasicrystal include Al-based transition metal alloys (TM alloys: AlMn, AlMnSi, AlCuFe, and AlPdMn); alloys having similar composition to that of the Frank–Kasper phase with tetrahedrally close-packed structure (FK alloys: Al-Cu-Li, Zn-Mg-RE; RE = rare earth); and stable binary alloys (Cd alloys: $Cd_{5.7}Yb$ and $Cd_{17}Ca_3$). One can observe a decagonal phase with a diffraction pattern of 10-fold rotational symmetry in AlMn, AlFe, AlCuCo, and AlCoNi. There is a one-dimensional translational periodicity along the 10-fold rotational axis in these alloys. CrNiSi and VNiSi are two-dimensional octagonal quasicrystals. The two-dimensional dodecagonal quasicrystals are TaTe and a polymer alloy.

### 17.5.4 Quasiperiodic Lattice

The various methods used to mathematically generate the structures of quasicrystals include the inflation–deflation operation, utilization of matching rules, grid method, strip projection method, cut projection method, or generalized dual method. We will discuss the strip projection method and note that the other methods are closely related.

In the strip projection method, the lattice points in the hypercubic lattice in the $n$-dimensional space $\mathbf{E}''$ are projected on vertices in the $d$-dimensional quasiperiodic lattice. $\mathbf{E}''$ is decomposed into two subspaces,

$$\mathbf{E}'' = \mathbf{E}^{\parallel} + \mathbf{E}^{\perp}, \tag{17.31}$$

where the subspace $\mathbf{E}^{\parallel}$ is the $d$-dimensional physical space, and $\mathbf{E}^{\perp}$ is orthogonal to $\mathbf{E}^{\parallel}$. $\mathbf{E}^{\perp}$ is called the "perpendicular space" (perp-space). The projection of a unit "hypercube" onto $\mathbf{E}^{\perp}$ is known as the "window" $\mathbf{W}$. For any $\mathbf{x}_0$ in $\mathbf{E}^{\parallel}$, we write $\mathbf{W}_0$ for $\mathbf{W} + \mathbf{x}_0$. When a lattice point in $\mathbf{E}''$ is located inside $\mathbf{W}_0$, its projection onto $\mathbf{E}^{\parallel}$ is selected as a vertex in the physical space $\mathbf{E}^{\parallel}$. If the "slope" of the hyperplane $\mathbf{E}^{\parallel}$ is rational to the hypercubic lattice in $\mathbf{E}''$, the projected lattice is periodic. However, if the "slope" of the hyperplane $\mathbf{E}^{\parallel}$ is irrational, the projected lattice becomes quasiperiodic. The hypercubic lattice, the directions of the two orthogonal subspaces $\mathbf{E}^{\parallel}$ and $\mathbf{E}^{\perp}$, and $\mathbf{W}$ must be invariant under operations of the noncrystalline group of the quasicrystal.

In Figure 17.15, we show a one-dimensional quasiperiodic lattice obtained by projection from a two-dimensional square lattice. The Fibonacci lattice is generated when the $\mathbf{E}^{\parallel}$-axis is generated at $\theta = \arctan 1/\tau$ to the $x$-axis. Here, the golden mean $\tau = (\sqrt{5}+1)/2$.

In Figure 17.16, we show a Fibonacci lattice, obtained in this manner, that can also be described as a one-dimensional section $(d = 1)$ of a two-dimensional periodic function $(N = 2)$. The two-dimensional periodic structure consists of a periodic arrangement of a line segment extending in the direction of $E_{\perp}$. The line segment is called an atomic surface. A point sequence is obtained on the $E_{\parallel}$ section comprised of two spacings $L$ and $S$. The irrational shape indicates the lack of periodicity in the arrangement of $L$ and $S$.

The distribution function of lattice points $\rho(\mathbf{x})$ of a two-dimensional square lattice is given by

$$\rho(\mathbf{x}) = \rho(x^{\parallel}, x^{\perp}) = \sum_{jl} \delta(x^{\parallel} - j\cos\theta - l\sin\theta) \times \delta(x^{\perp} + j\sin\theta - l\cos\theta), \tag{17.32}$$

and the distribution function on the projected lattice on $\mathbf{E}^{\parallel}$ is (Problem 17.8)

$$\rho_0(x^{\parallel}) = \int_{-\infty}^{\infty} dx^{\perp} \rho(x^{\parallel}, x^{\perp}) W(x^{\perp}). \tag{17.33}$$

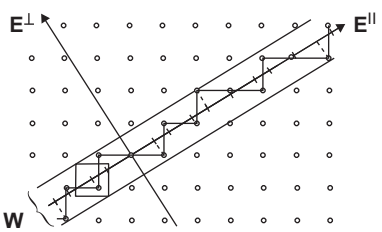


**FIGURE 17.15**

One-dimensional quasiperiodic lattice (crossmarks on the $\mathbf{E}^{\parallel}$-axis) generated by projection.

*Reproduced from Misra[18] with the permission of Elsevier.*

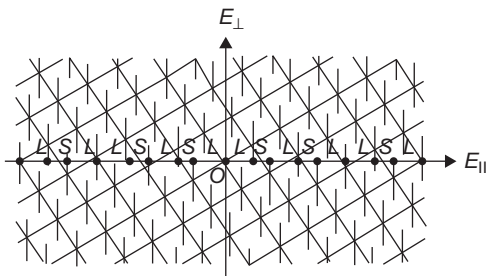


**FIGURE 17.16**

A Fibonacci lattice.

*Reproduced from Misra[18] with the permission of Elsevier.*

Here,

$$W(x^{\perp}) = \begin{cases} 1, & \text{if } 2|x^{\perp}| < (\cos\theta + \sin\theta) \\ 0, & \text{otherwise.} \end{cases} \tag{17.34}$$

The diffraction pattern of the one-dimensional Fibonacci lattice is expressed by a structure factor

$$\begin{aligned} f(k) &= \int_{-\infty}^{\infty} dx^{\parallel} e^{-ikx^{\parallel}} \rho_0(x^{\parallel}) \\ &\approx \sum_{m,n=-\infty}^{\infty} \frac{\sin k^{\perp}\omega}{k^{\perp}\omega} \delta(k - 2\pi(m\,\sin\theta + n\cos\theta)). \end{aligned} \tag{17.35}$$

Here,

$$\omega = \frac{1}{2}(\cos\theta + \sin\theta) \tag{17.36}$$

and

$$k^{\perp} = 2\pi(m\cos\theta + n\cos\theta). \tag{17.37}$$

This procedure of projection and calculation of structure factor is generalized to higher-dimensional cases. For example, the pentagonal quasicrystal is obtained by a projection of the hypercubic lattice to a two-dimensional space and the icosahedral quasicrystal by that of the six-dimensional one to a three-dimensional space. The three-dimensional icosahedral quasicrystals are constructed by two rhombohedral units: prolate and oblate.

### 17.5.5 Phonon and Phason Degrees of Freedom

The diffraction intensity pattern $I(\mathbf{q})$ of a solid is, in general, given by

$$I(\mathbf{q}) \equiv |S(\mathbf{q})|^2, \tag{17.38}$$

where

$$S(\mathbf{q}) = \int \rho(\mathbf{r}) e^{-2\pi i \mathbf{q}\cdot\mathbf{r}} d\mathbf{r}, \tag{17.39}$$

$\mathbf{q}$ is the wave vector, and $\rho(\mathbf{r})$ is the atomic-density function in real space. For a quasicrystal, the characteristics of the function $I(\mathbf{q})$ observed experimentally are as follows:

**a.** It consists of $\delta-$ functions.
**b.** The number of basis vectors necessary for indexing the positions of the $\delta-$ functions exceeds the number of dimensions.
**c.** It shows a rotational symmetry forbidden in the conventional crystallography.

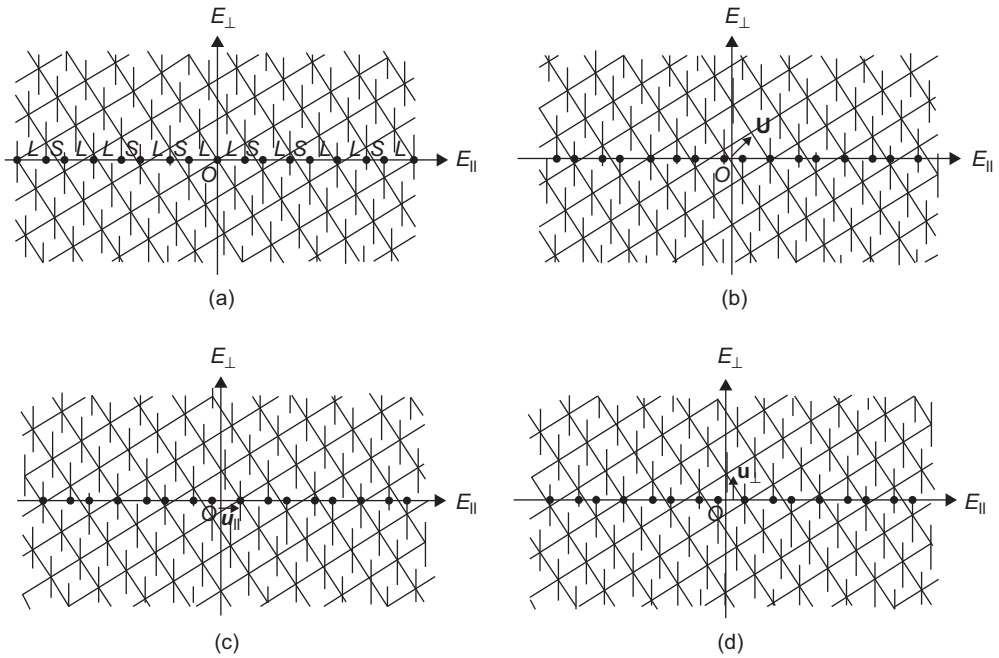


**FIGURE 17.17**

(a) A Fibonacci lattice, the structure resulting from a displacement of (b) **U**, (c) **u**, and (d) **w**.

*Reproduced from Misra[18] with the permission of Elsevier.*

As an example, we consider the Fibonacci lattice in Figure 17.17a. We consider the translation of the two-dimensional periodic structure by a vector **U** with respect to the origin of the physical space $E_\parallel$ (Figure 17.17b). It can be shown that the two structures on $E_\parallel$ before and after the displacement **U** can be overlapped out to large finite distances by a finite translation in $E_\parallel$. These two structures are said to belong to the same local isomorphic class (LI class). Because these structures are physically indistinguishable, they give the same diffraction intensity function I(**q**) and have the same energy. The vector **U** can be written as

$$\mathbf{U} = \mathbf{u} + \mathbf{w}, \tag{17.40}$$

where **u** represents the degrees of freedom of $d$-dimensional translation in physical space that crystals also possess, and **w** represents $(N-d)$ degrees of freedom characteristic of a quasiperiodic system. Figure 17.17c shows **u** results in a translation of the Fibonacci lattice in $E_\parallel$, and Figure 17.17d shows how **w** generates a rearrangement of $L$ and $S$.

Here, **u** and **w** are called phonon and phason displacements. When these displacements vary spatially, their gradients yield a strain. The gradient of **u** yields the conventional elastic strain (phonon strain), whereas the gradient of **w** yields the phason strain. A phonon-strained Fibonacci lattice is shown in Figure 17.18. A uniform phonon strain is introduced by a compression deformation of the two-dimensional structure.

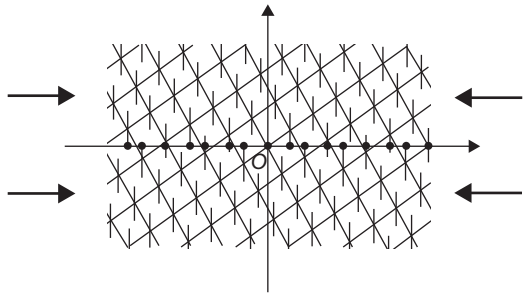


**FIGURE 17.18**

Phonon-strained Fibonacci lattice.

*Reproduced from* Misra[18] *with the permission of Elsevier.*

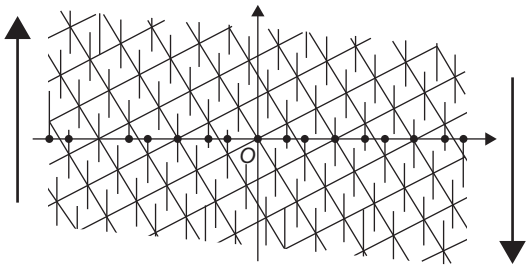


**FIGURE 17.19**

Phason-strained Fibonacci lattice.

*Reproduced from Misra*[18] *with the permission of Elsevier.*

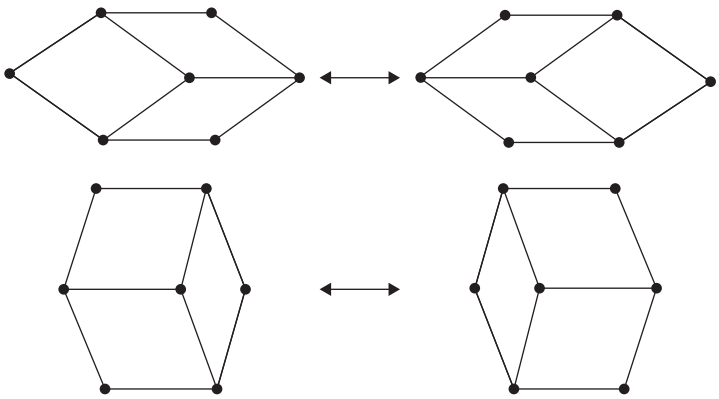

**FIGURE 17.20**

Examples of phason flips in the two-dimensional Penrose lattice.

*Reproduced from Misra*[18] *with the permission of Elsevier.*

A uniform phason strain is introduced by a shear deformation of the Fibonacci lattice, as shown in Figure 17.19.

A phason displacement results in a local rearrangement of points (atoms) such as $LS \leftrightarrow SL$, which is known as the phason flip. Examples of the phason flip in two-dimensional Penrose lattice, which is known as a two-dimensional decagonal quasicrystal, are shown in Figure 17.20.

To decompose properly the total $N$ degrees of freedom into $d$ phonon and $(N-d)$ phason degrees of freedom, i.e., to embed properly a given $d$-dimensional quasiperiodic structure into an $N$-dimensional hypercrystal, one needs to know the point group symmetry of the system.

### 17.5.6 Dislocation in the Penrose Lattice

The perfect edge dislocation introduced in the two-dimensional Penrose lattice (or Penrose tiling) is shown in Figure 17.21. The phason strain field cannot be easily recognized around the dislocation. However, the tiling pattern changes when the dislocation position is translated to the left by a distance represented by the arrow.

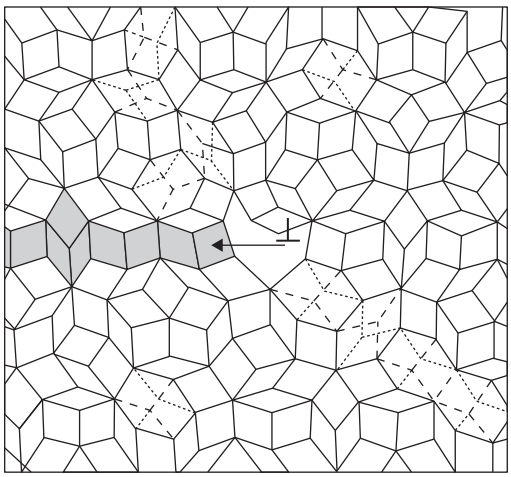

**FIGURE 17.21**

A perfect edge dislocation in the Penrose lattice. The shaded tiles are destroyed to produce intratile phason defects after gliding the dislocation to the left.

*Reproduced from Misra[18] with the permission of Elsevier.*

### 17.5.7 Icosahedral Quasicrystals

An icosahedron, shown in Figure 17.22, is a regular polyhedron with 20 identical equilateral triangular sides. The main characteristics of a quasicrystal structure are that it is a combination of a quasiperiodic lattice and a cluster decorating it. Three types of icosahedral quasilattices, P-, F-, and I-types, are known theoretically, out of which two types, P and F, have been observed experimentally. These two types are distinguished by reflection conditions.

The reflection vector of $\mathbf{g}$ of a icosahedral quasicrystal can be written as

$$\mathbf{g} = \frac{1}{a_{6D}} \sum_{1}^{6} \mathbf{m}_i \mathbf{e}_{i//}, \qquad (17.41)$$

where the six $\mathbf{e}_{i//}$ vectors with length 1/2 are parallel to the lines connecting to the center and vertices of an icosahedron, and $a_{6D}$ is the lattice parameter of the six-dimensional hypercubic lattice in the framework of the section. There are no restrictions for the indices in the case of P-type reflections, whereas either all odd or all even indices appear in the F-type. The reflection condition in the F-type exhibits a $\tau$-scaling rule ($\tau$: golden mean), whereas the P-type has a $\tau^3$-scaling rule. However, in real space, a P-type quasilattice can be decomposed into two F-type sublattices. Thus, the F-type quasicrystal can be interpreted as an ordered phase, in which two kinds of atomic clusters with different atomic configurations are arranged regularly.

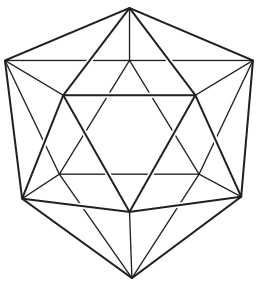

**FIGURE 17.22**

The icosahedron.

In the case of Al-transition metal quasicrystals, the Mackay-type cluster is considered as a basic structural unit. The 54 atoms form the triple shells as presented in Figure 17.23a. The first and the

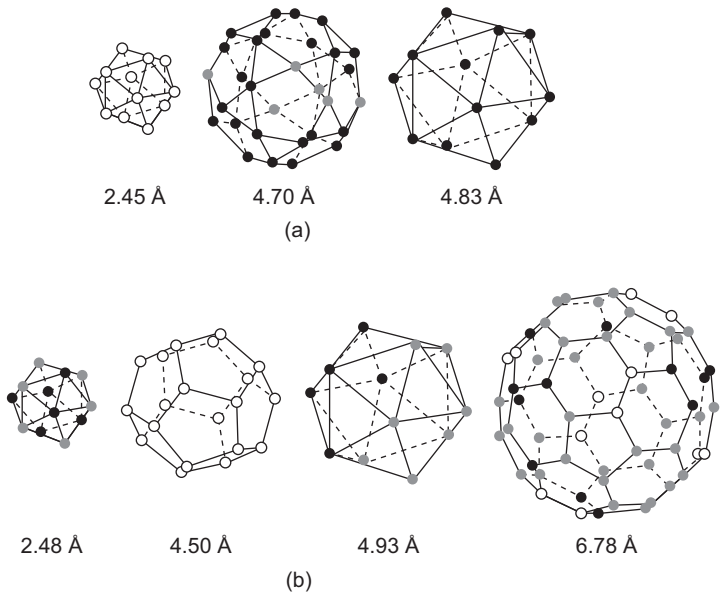


**FIGURE 17.23**

Icosahedral atomic clusters. (a) Mackay type in Al-Mn-Si approximant and (b) Bergman type in Zn-Mg-Al approximant. The radius in each shell is inserted.

*Reproduced from Misra[18] with the permission of Elsevier.*

second shell, which are composed of Al, are an icosahedron and an icosidodecahedron, respectively. The third shell is a larger icosahedron of the transition metal. The five ternary alloys, which are of the stable Mackay type, are Al-Cu-(Fe, Ru, Os) and Al-Pd-(Mn, Re).

The Zn-based quasicrystals are the Bergman clusters shown in Figure 17.23b. They include 104 atoms. This cluster has four concentric shells: an icosahedron, a dodecahedron, a larger icosahedron, and a truncated icosahedron (soccer ball). The 10 ternary alloys, which are of the Bergman type, are Al-Li-Cu, Zn-Mg-Ga, Ti-Zr-Ni, Mg-Al-Pd, and Zn-Mn-(Y, Dy, Gd, Ho, Tb, and Er).

## 17.6 AMORPHOUS SOLIDS

### 17.6.1 Introduction

Amorphous solids have attracted a great deal of attention in recent years. There are an infinite number of ways in which the geometrical arrangement of atoms can be visualized. Sometimes, amorphous solids have been visualized as frozen-liquid structures, but there are some significant differences between the two types of states. For example, there are distinct differences between the radial distribution of functions for a true liquid and an amorphous solid. Another interesting difference in their properties is that whereas liquid Ge and Si are metals, amorphous Si and Ge

are semiconductors. The bonds are broken in liquid Ge and Si, where presumably the $sp^3$ configuration in the solid is changed to an $s^2p^2$ configuration in the liquid, which makes it metallic. However, in the amorphous state, the $sp^3$ bonds are still present between nearest neighbors. These bonds are imperfect because the amorphous films are produced at relatively low temperature. Due to this bonding, amorphous Ge and Si are semiconductors like their crystalline counterpart, but there are significant differences arising out of the fact that (1) the bonding is imperfect because there is no true tetrahedral symmetry in spite of four-fold coordination over small regions; (2) different regions are not linked because there is no long-range order; and (3) many atoms could have only three nearest neighbors due to which the bond angles are severely distorted from the ideal value.

Amorphous solids can be obtained in a variety of ways. In some cases, they are obtained in the frozen-liquid amorphous state either by evaporation into a cooled substrate or by extremely rapid cooling from the melt. The more popular method is by a process known as "sputtering" the components onto a cooled substrate. In this process, the atoms in a solid are knocked out by energetic ions of inert gas such as argon. The inert gas is at a reduced pressure. It is ionized by an electrical discharge. A substrate is placed above the solid, which is in contact with an electrode, and the atoms are discharged by the impingement of the energetic argon ionized by the electric discharge. The atoms condense above the substrate and form a thin film. The sputtering process has the advantage that a thin layer of an amorphous film is deposited on the substrate. The disadvantage of this method is that both argon and oxygen are invariably present as impurities.

### 17.6.2 Energy Bands in One-Dimensional Aperiodic Potentials

To consider the localized states, we consider the energy bands in one-dimensional aperiodic potentials.[8] We consider a finite segment of a line $a < x < b$, where $b - a = L$. The potential energy of the segment is periodic but can be derived from a periodic potential by a disordering process. The two linearly independent real solutions of the Schrodinger equation are

$$\int_a^b \psi_1^2 dx = 1, \quad \text{where } \psi_1(a) = \psi_1(b), \tag{17.42}$$

and

$$\int_a^b \psi_1(x)\psi_2(x)dx = 0, \quad \int_a^b \psi_2^2(x)dx = 1. \tag{17.43}$$

Economou and Cohen (Ref. 8) postulated that the solutions of the aperiodic case that most resemble the Bloch functions of the periodic case are those combinations of $\varphi$ that satisfy an extremal condition in relation to the average value of momentum $<\hat{p}>$. $\varphi$ is so chosen that the real part of $<\hat{p}>$ is as extremum. One can write $\varphi$ as

$$\varphi = \psi_1 + (\alpha + i\beta)\psi_2/[1 + \alpha^2 + \beta^2]^{\frac{1}{2}}, \tag{17.44}$$

where $x$ and $y$ are real. The average value of $\hat{p}$ (Problem 17.9) is

$$<\hat{p}> = -i\hbar \int \varphi^*(d\varphi/dx)dx = \hbar \frac{\beta(\pi_{12} - \pi_{21}) - i[\pi_{11} + (\alpha^2 + \beta^2)\pi_{22} + \alpha(\pi_{12} + \pi_{21})]}{1 + \alpha^2 + \beta^2}, \tag{17.45}$$

where

$$\pi_{ij} = \int_a^b \psi_i d\psi_j, \quad i,j = 1,2\,. \tag{17.46}$$

The extremum requirement on Re $<\hat{p}>$ gives

$$\alpha = 0,\ \beta = 1 \text{ or } \alpha = 0,\ \beta = -1. \tag{17.47}$$

To avoid obtaining the nonzero imaginary part of the expectation value of the extremum value of $<\hat{p}>$ from the preceding solutions, Economou and Cohen imposed periodic boundary conditions,

$$\psi_2(a) = \psi_2(b), \tag{17.48}$$

so that the energy eigenvalues originating from Eq. (17.48) are exactly the same as the first, third, fifth, and so on, obtained by setting $V = \infty$ outside $(a, b)$. Thus, there are half the number of values in this problem as in the infinite-barrier problem.

From Eqs. (17.44) and (17.47), there are two functions that make $<\hat{p}>$ an extremum (Problem 17.10),

$$\varphi = (\psi_1 + i\psi_2)/\sqrt{2} \tag{17.49}$$

and

$$\varphi^* = (\psi_1 - i\psi_2)/\sqrt{2}. \tag{17.50}$$

The corresponding values of $<\hat{p}>$ are

$$p_{ext} = \pm\frac{1}{2}\hbar(\pi_{12} - \pi_{21}) = \pm\hbar\pi_{12}. \tag{17.51}$$

One can easily show that the set of functions $\varphi_n(x), \varphi_n^*(x)$, $n = 1, 2, 3, \ldots$ is complete and orthonormal and makes each momentum expectation value extremal. This set is the closest one can come to a set of Bloch functions in the aperiodic case. A schematic representation of these results is shown in Figure 17.24. Here, $E_c$ is the energy at which the states change from localized to extended. $E_B$ is the energy at which the density of states vanishes, the bound of the spectrum. They coincide in the periodic case and move in the opposite direction as the aperiodicity is increased.

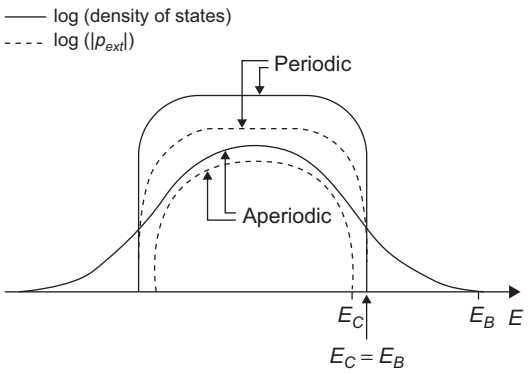


**FIGURE 17.24**

Density of states (solid curve) and distribution of the extended states (dashed curve) for an energy band of an ordered and disordered lattice.

*Reproduced from Economou and Cohen (Ref. 8)* with the permission of the American Physical Society.

### 17.6.3 Density of States

Concepts such as crystal momentum, effective mass, or band structure function E(**k**) cannot be used for localized one-electron states. However, the concept that is used and still valid is the density of states, $g(E)$, which can be defined as

$$g(E) = \frac{1}{V_g}\sum_i \delta(E - E_i). \tag{17.52}$$

In delocalized states of disordered solids, bands can exist in which tails with localized states are attached to their edges. The region without states between the tails of two adjacent bands is called a gap, or if the tails overlap, the region is known as a pseudogap.

### 17.6.4 Amorphous Semiconductors

We first assume that each Ge or Si atom in the amorphous state has four nearest neighbors as in the crystalline state. However, the covalent bonds in the crystalline phase are distorted in the amorphous phase. The band edges of the conduction and valence band contain localized states. They are separated from the extended states by the mobility edges. The abrupt band edges are shown in Figure 17.25.

The electrons occupying the tail states cannot take part in the conduction because they are localized due to the disorder in the potential.

Normally, each Si or Ge atom, which has four valence electrons, shares one electron in the covalent bond with its neighbor. However, in the amorphous state, the three-fold-coordinated atoms produce a dangling bond because one bond remains uncompensated. A dangling bond essentially means an electron and an empty state. The electron in the dangling bond is localized at 0° K because there are no adjacent sites available for it to move in the amorphous state. The concentration of these dangling bonds is very high (on the order of $10^{25}\text{m}^{-3}$), and they control the position of the Fermi level.

However, at finite temperatures, the process of electrical conduction occurs in three different regimes: the propagating regime, the jumping regime, and the hopping regime. The propagating regime, which is commonplace in the crystalline solid state theory, is dominant in disordered systems only at very high temperatures. At intermediate temperatures, electronic conduction in such systems takes place by diffusion or Brownian motion. This type of conduction, encountered near the mobility edges of amorphous solids, is known as jumping conduction. At low temperatures, the hopping regime is prevalent. In this regime, the electrons can move only through phonon-assisted hopping. At relatively higher temperatures in the hopping regime of conduction, the largest tunnel contribution arises from jumps to unoccupied levels of nearest-neighbor centers. At lower temperatures, the number and

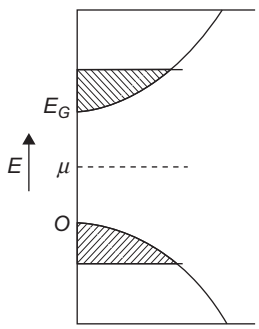


**FIGURE 17.25**

Localized states at the edges of the valence and conduction bands in amorphous semiconductors.

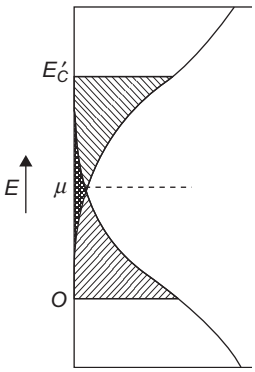


**FIGURE 17.26**

The overlap of the tails of the localized states in amorphous tetrahedral semiconductors.

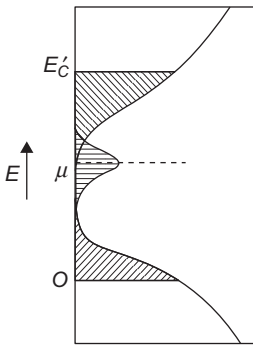


**FIGURE 17.27**

Impurity band of local defects in the gap or the pseudogap.

energy of phonons available for absorption decrease so that tunneling is restricted to seek centers that are not nearest neighbors but lie energetically closer. This type of conduction is known as variable-range hopping.

The overlap of tails of the localized states in amorphous tetrahedral semiconductors is shown in Figure 17.26.

The regime of variable-range hopping is subdivided into two ranges. At relatively higher temperatures of this regime, variable-range hopping transport is done by tunneling conduction in a band tail with somewhat large activation energy. At the lower temperature range, hopping transport by tunneling conduction near the Fermi level is favored.

The local defects, such as dangling bonds, can cause impurity bands to appear in the gap or pseudogap. This is shown in Figure 17.27.

The extended states above the mobility gap are important in deciding the optical properties. However, at low temperatures, the transport properties of amorphous semiconductors are mainly determined by the states of the local defects rather than the localized states of the tail states.

## PROBLEMS

**17.1.** Show that in a region where $|\chi_0|$ is everywhere nonzero, the application of the Stokes theorem to the curl of Eq. (17.14) leads to the conclusion that the integral of $v_s$ around any closed curve is zero.

**17.2.** Show that when we integrate Eq. (17.14) around a circuit that encloses the one-dimensional region, the fact that the phase of the wave function $\chi_0$ must be single-valued modulo $2\pi$ leads to the Onsager–Feynman quantization condition

$$\oint v_s \cdot dl = nh/m. \tag{1}$$

**17.3.** Show that because, in the range of temperatures above 0.01° K, the nuclear spins of the $^3$He atoms comprising the solid are almost fully disordered, the entropy $S_{solid} = R \ln 2$ (per mole).

**17.4.** The dipolar interaction is calculated by taking a quantum mechanical average of the dipolar Hamiltonian over the order parameter (pair-wave function). It can be shown that the dipolar free energies are given by

$$\Delta F_D = \begin{cases} -\frac{3}{5} g_D(T)[1 - \vec{d} \cdot \vec{l})^2], & A \text{ phase}, \\ \frac{4}{5} g_D(T)\left\{\cos\theta + 2\cos^2\theta + \frac{3}{4}\right\}, & B \text{ phase}, \end{cases} \tag{1}$$

where

$$g_D \approx \left(1 - \frac{T}{T_c}\right) 10^{-3} \text{ergs/cm}^3. \tag{2}$$

Show that to minimize the free energy, $\vec{l}$ and $\vec{d}$ must be parallel in the $A$ phase, and the dipolar energy is minimized for $\theta = \cos^{-1}(-\frac{1}{4}) = 104°$ in the $B$ phase.

**17.5.** For a nematic or cholesteric liquid crystal where the molecules are rigid and rodlike in shape, the order parameter can be expressed as a second-rank tensor

$$S_{\alpha\beta}(\mathbf{r}) = \frac{1}{N} \sum_i \left( v_\alpha^{(i)} v_\beta^{(i)} - \frac{1}{3} \delta_{\alpha\beta} \right), \tag{1}$$

where the sum is over all the $N$ molecules in a macroscopic volume located at $\mathbf{r}$, and the $v_\alpha$ are the components of $\vec{v}$ referred to by a set of laboratory-fixed axes. Show that in the isotropic case, where the molecules have random orientation, $S_{\alpha\beta} = 0$.

**17.6.** In the order parameter for nonlinear rigid molecules, one can introduce a Cartesian coordinate system $x'y'z'$ fixed in the molecules. In the case of a uniaxial liquid crystal, the order parameter tensor is defined by

$$S_{\alpha'\beta'}(\mathbf{r}) = < \cos\theta_{\alpha'} \cos\theta_{\beta'} - \frac{1}{3} \delta_{\alpha'\beta'} >, \tag{1}$$

where $\cos\theta_{\alpha'}$ is the angle between the $\alpha'$ molecular axis, and the preferred direction or the optic axis. The angle brackets indicate an average over the molecules in a small but macroscopic volume. Show that Eq. (1) in Problem (17.6) is equivalent to Eq. (1) in Problem (17.5) in the case of linear molecules or molecules with a well-defined long axis about which they rotate rapidly.

**17.7.** Show that for a uniaxial liquid crystal,

$$Q_{xx} = Q_{yy} = 2N[(S_{y'y'} + S_{z'z'})\chi_1^{(0)} + (S_{z'z'} + S_{x'x'})\chi_2^{(0)} + (S_{x'x'} + S_{y'y'})\chi_3^{(0)}] \tag{1}$$

and

$$Q_{zz} = N(S_{x'x'}\chi_1^{(0)} + S_{y'y'}\chi_2^{(0)} + S_{z'z'}\chi_3^{(0)}), \tag{2}$$

where $N$ is the number of molecules per unit volume where the symbols are defined in the text.

**17.8.** In a quasicrystal, the distribution function of lattice points $\rho(\mathbf{x})$ of a two-dimensional square lattice is given by

$$\rho(\mathbf{x}) = \rho(x^{\parallel}, x^{\perp}) = \sum_{jl} \delta(x^{\parallel} - j\cos\theta - l\sin\theta) \times \delta(x^{\perp} + j\sin\theta - l\cos\theta). \tag{1}$$

Show that the distribution function on the projected lattice on $\mathbf{E}^{\parallel}$ is

$$\rho_0(x^{\parallel}) = \int_{-\infty}^{\infty} dx^{\perp} \rho(x^{\parallel}, x^{\perp}) W(x^{\perp}). \tag{2}$$

Here,

$$\begin{aligned} W(x^{\perp}) &= \begin{cases} 1, & \text{if } 2|x^{\perp}| < (\cos\theta + \sin\theta) \end{cases} \\ &= \begin{cases} 0, & \text{otherwise.} \end{cases} \end{aligned} \tag{3}$$

**17.9.** Show that if one writes $\varphi$ as

$$\varphi = \psi_1 + (\alpha + i\beta)\psi_2 / [1 + \alpha^2 + \beta^2]^{\frac{1}{2}}, \tag{1}$$

where $x$ and $y$ are real, the average value of the momentum $\hat{p}$ is

$$<\hat{p}> = -i\hbar \int \varphi^*(d\varphi/dx)dx = \hbar \frac{\beta(\pi_{12} - \pi_{21}) - i[\pi_{11} + (\alpha^2 + \beta^2)\pi_{22} + \alpha(\pi_{12} + \pi_{21})]}{1 + \alpha^2 + \beta^2}, \tag{2}$$

where

$$\pi_{ij} = \int_a^b \psi_i d\psi_j, \quad i, j = 1, 2\,. \tag{3}$$

**17.10.** Show from Eqs. (17.44) and (17.47) that the two functions that make $<\hat{p}>$ an extremum are

$$\varphi = (\psi_1 + i\psi_2)/\sqrt{2} \tag{1}$$

and

$$\varphi^* = (\psi_1 - i\psi_2)/\sqrt{2}. \tag{2}$$

## References


1. Anderson PW, Morel P. Generalized Bardeen-Cooper-Schrieffer States and the proposed low-temperature Phase of Liquid He3. *Phys Rev* 1961;**123**:1911.
2. Anderson PW, Brinkman WF. Anisotropic Superfluidity in He3: A Possible Interpretation of its Stability as a Spin-Fluctuation Effect. *Phys Rev Lett* 1973;**30**:1108.
3. Ashcroft NW, Mermin ND. *Solid state physics*. New York: Brooks/Cole; 1976.
4. Balian R, Werthamer NR. *Phys. Rev.* 1963;**131**:1553. Superconductivity with Pairs in a Relative p Wave.
5. Barker JA, Henderson DH. What is "liquid"? Understanding the states of matter. *Rev Mod Phys* 1976;**48**:587.
6. Chandrasekhar S. *Liquid Crystals*. Cambridge: Cambridge University Press; 1992.
7. de Gennes P-G, Prost J. *The physics of liquid crystals*. Oxford: Clarendon Press; 1993.
8. Economou EN, Cohen MH. Energy Bands in One-Dimensional Aperiodic Potential. *Phys Rev Lett* 1970;**24**:218.
9. Kramer P. Non-periodic Central space filling with icosahedral symmetry using copies of seven elementary cells. *Acta Crystallogr* 1982;**A38**:257.
10. Landau LD. *J Phys.* USSR 1941;**5**:71.
11. Landau LD. *JETP* 1957;**3**:920.
12. Landau LD. *JETP* 1957;**5**:101.
13. Landau LD, Lifshitz EM. *Statistical physics, part 1*. Oxford: Pergamon Press; 1980.
14. Lee DM. The Extraordinary phases of liquid He3. *Rev Mod Phys* 1997;**69**:645.
15. London F. On the Bose-Einstein Condensation. *Phys Rev* 1938;**54**:947.
16. Mackay AL. Cryatallography and the Penrose patterns. *Physica* 1982;**114A**:609.
17. Marder MP. *Condensed matter physics*. New York: John Wiley & Sons; 2000.
18. Misra PK, Fujiwara T, Ishii Y. *Quasicrystals*. Amsterdam: Elsevier; 2008.
19. Mott NF, Davis EA. *Electronic properties of noncrystalline materials*. Oxford: Clarendon Press; 1979.
20. Osheroff DD, Richardson RC, Lee DM. Evidence for a New Phase of Solid He3. *Phys Rev Lett* 1972;**28**:885.
21. Osheroff DD, Gully WJ, Richardson RC, Lee DM. New magnetic Phenomena in Liquid He3 below 300 K. *Phys Rev Lett* 1972;**29**:920.
22. Paulson DN, Kojima H, Wheatley JC. Preferred Effect of a Magnetic Field in the Phase Diagram of Superfluid 3He. *Phys Rev Lett* 1974;**32**:1098.
23. Penrose R. *Bull Inst Math Appl* 1974;**10**:266.
24. Shechtman D, Blech L, Gratias D, Cahn JW. Metallic Phase with Long Range Orientational Order and no Translational Symmetry. *Phys Rev Lett* 1984;**53**:1951.
25. Stephen MA, Straley JP. Physics of Liquid Crystals. *Rev Mod Phys* 1974;**46**:617.
26. Webb RA, Greytak JT, Johnson RT, Wheatley. Observation of a second-order Phase Transition and its Associated P-T phase Diagram in liquid He3. *Phys Rev Lett* 1973;**30**:210.